Thermodynamic model for solid-state amorphization in binary systems at interfaces and grain boundaries

R. Benedictus,* A. Böttger, and E. J. Mittemeijer
Laboratory of Materials Science, Delft University of Technology, Rotterdamseweg 137, 2628 AL Delft, The Netherlands
(Received 30 October 1995)

A thermodynamic model for solid-state amorphization (SSA) at interfaces and grain boundaries in binary systems has been proposed. It has been demonstrated that the energy of a crystalline-amorphous interface is, in general, lower than the energy of a crystalline-crystalline interface. This effect provides the driving force for SSA, as long as the amorphous product layer is not too thick. The model has been applied to several binary crystalline-crystalline systems and binary crystalline-amorphous systems to predict whether or not interface and/or grain boundary amorphization can occur and to calculate the maximum thickness of the amorphous layer. The results obtained agree with experimental data reported in the literature. [S0163-1829(96)05838-9]

I. INTRODUCTION

At the interface of certain crystalline binary metal-metal (A-B) systems an amorphous phase can form by interdiffusion. Since the initial discovery of this solid-state amorphization (SSA)[1] the list of binary metal-metal diffusion couples exhibiting this type of reaction numbers in the dozens. Usually such diffusion couples are composed of an early transition metal and a late transition metal (e.g., Ni-Ti, Ni-Zr) or of a metal and (amorphous) Si.[2] SSA is of great technological interest because of its potential application to produce amorphous bulk products and coatings of metallic amorphous phases (for example, useful as diffusion barriers). Also SSA may occur as an ageing-induced artifact in semiconductor devices.

Although research on SSA is focused usually on amorphization along the original interface between the two parent crystalline phases, it was recently shown that grain boundaries in one of the crystalline phases (A or B), in contact with the (A/B) interface, provide sites where amorphization can occur, in addition to amorphization at the interface.[3,4] Grain boundaries in crystalline solids provide trajectories along which diffusion takes place usually much faster than in the bulk of the crystals. In as far as diffusion plays a rate limiting role in the SSA process, it may thus be expected that the amorphous phase also grows at the grain boundaries within the sublayers of the parent crystalline phases. Also, in as far as the initiation of SSA is a nucleation controlled process, it may be expected that an amorphous phase can be nucleated preferentially at the junction of the interface and the grain boundary. Until now grain-boundary amorphization has been reported for a few systems only: Ni-Ti,[3,4] Ni-Zr,[5] Cu-Y,[6] and Ti-Si.[7]

From a scientific point of view, research on SSA may provide insight into the thermodynamics and the kinetics of the formation of metastable phases. Originally, two conditions for SSA to occur, have been indicated:[1] there should be a thermodynamic driving force (negative Gibbs free energy of mixing of A and B) and the formation of the more stable crystalline intermetallic compound should be kinetically hindered.

A thermodynamic analysis of SSA involves comparison of the volume (bulk) Gibbs free energies of the amorphous product phase and the parent crystalline phases, and of the associated interfacial energies; cf. wetting and premelting phenomena of grain boundaries and surfaces.[8] In general an interface between a crystalline and an amorphous phase has a lower energy than an interface between two crystalline phases (as will be shown in Sec. IV). Therefore, it can be anticipated that in the initial stage of SSA, the change in interface energy can provide a contribution to the driving force for SSA, that can be large as compared to the mixing energy. This change in nature of the interface is also the reason why, on a crystalline substrate, a thin amorphous layer can be more stable than a thin crystalline layer (see Sec. IV).

Until now only a very crude estimate of the average interfacial energy between two metals has been used in an approximation for the Gibbs free energy change upon amorphization.[9,10] In this paper a material composition dependent expression for the interface energies will be applied on the basis of the Miedema model.[11] The Miedema model can be used beneficially also because for almost all metals the relevant thermodynamic data are available (see, e.g., Ref. 11).

The thermodynamic model proposed in this paper (Secs. II and III) describes the Gibbs free energy effects of interface SSA and grain-boundary SSA and leads to the criteria for the occurrence of these processes. The model can be applied easily and successfully to binary systems, as is illustrated by comparison with experimental results on SSA published previously (Secs. VI and VII).

II. SOLID-STATE AMORPHIZATION AT INTERFACES

In the following study of the thermodynamics of SSA a symmetric diffusion couple is taken (see Fig. 1). Such a diffusion couple can be considered as the representative unit cell of a multilayer (most of the research about SSA is per-

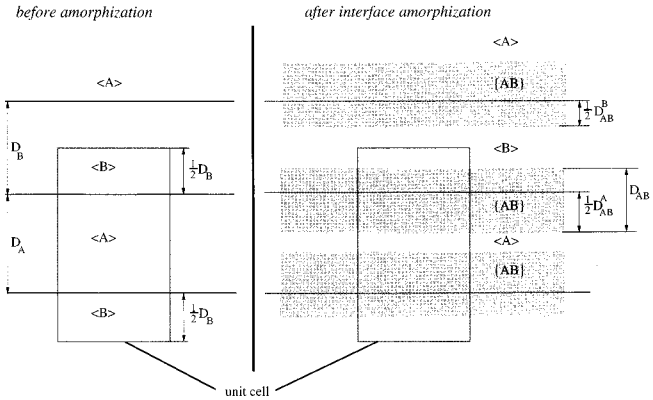

FIG. 1. Schematic drawing of an A-B multilayer before and after amorphization at the A/B interface. The symbol $\langle\ \rangle$ refers to the crystalline phase and the symbol $\{\ \}$ refers to the amorphous phase. D_A and D_B are the initial thicknesses of the crystalline phases $\langle A\rangle$ and $\langle B\rangle$, respectively. The total thicknesses of the amorphous layers grown in layer A and layer B, are denoted by D^A_{AB} and D^B_{AB}, respectively. The thermodynamics of interface amorphization are calculated for a unit cell of lateral area of 10×10 nm^2 and with a height equal to the sum of D_A ($=10$ nm) and D_B ($=10$ nm).

formed with multilayers), but the treatment to be presented here is applicable to all binary diffusion couples. A schematic drawing of a binary A-B multilayer before and after interface amorphization is given in Fig. 1. The driving force of interface SSA is provided by the difference of the Gibbs free energy after amorphization and the Gibbs free energy before amorphization. For simplicity it is assumed in the calculations that the composition of the amorphous phase is constant throughout the amorphous layer; this assumption does not affect the conclusions in an essential way. In this paper the following convention is applied: $\langle x\rangle$ refers to the solid crystalline phase x; $\{x\}$ denotes the amorphous phase x; γ indicates the interface energy with a subscript that refers to the type of interface.

The thermodynamics of interface amorphization will be described for a unit cell of volume (D_A+D_B) unit area as defined in Fig. 1, where D_A and D_B are the initial layer thicknesses of the crystalline phases $\langle A\rangle$ and $\langle B\rangle$, respectively. Before amorphization the unit cell consists of two crystalline phases with two interfaces ($\langle A\rangle-\langle B\rangle$ interfaces). Hence, the total Gibbs free energy of the unit cell before amorphization (G_i) consists of contributions of the Gibbs free energy of crystalline A ($G_{\langle A\rangle}$ per mole A), the Gibbs free energy of crystalline B ($G_{\langle B\rangle}$ per mole B) and the interface energy of the $\langle A\rangle-\langle B\rangle$ interfaces ($\gamma_{\langle A\rangle-\langle B\rangle}$ per unit surface):

$$G_i = D_A\,\frac{G_{\langle A\rangle}}{V_A} + D_B\,\frac{G_{\langle B\rangle}}{V_B} + 2\,\gamma_{\langle A\rangle-\langle B\rangle}, \tag{1}$$

where V_A and V_B are the molar volumes of $\langle A\rangle$ and $\langle B\rangle$, respectively. After interface amorphization the unit cell contains two crystalline phases, one amorphous phase, two $\langle A\rangle-\{AB\}$ interfaces and two $\langle B\rangle-\{AB\}$ interfaces. The total thicknesses of the amorphous layers grown in layer A and layer B, are denoted by D^A_{AB} and D^B_{AB}, respectively. The total Gibbs free energy of the unit cell after amorphization (G_e) is given by

$$G_e = (D_A - D^A_{AB})\,\frac{G_{\langle A\rangle}}{V_A} + (D_B - D^B_{AB})\,\frac{G_{\langle B\rangle}}{V_B} + (D^A_{AB}+D^B_{AB}) \times \frac{G_{\{AB\}}}{V_{AB}} + 2\,\gamma_{\langle A\rangle-\{AB\}} + 2\,\gamma_{\langle B\rangle-\{AB\}}, \tag{2a}$$

where $G_{\{AB\}}$ is the molar Gibbs free energy of the amorphous phase. For the present calculations it can be assumed that the molar volume of an amorphous phase is similar to the molar volume of a crystalline phase with the same composition ($V_{\{AB\}}\cong V_{\langle AB\rangle}\equiv V_{AB}$). Defining $\Delta G^f_{\{AB\}}$ as the Gibbs free energy of formation of $\{AB\}$, i.e., as the difference of the Gibbs free energy of the amorphous alloy $\{AB\}$ and the sum of the Gibbs free energies of the amounts of the crystalline phases $\langle A\rangle$ and $\langle B\rangle$ involved in $\{AB\}$ formation ($\Delta G^f_{\{AB\}}\equiv G_{\{AB\}} - cG_{\langle A\rangle} - (1-c)G_{\langle B\rangle}$, where c denotes the mole fraction of A in $\{AB\}$), Eq. (2a) can be rewritten as (cf. the Appendix)

$$G_e = D_A\,\frac{G_{\langle A\rangle}}{V_A} + D_B\,\frac{G_{\langle B\rangle}}{V_B} + 2D_{AB}\,\frac{\Delta G^f_{\{AB\}}}{V_{AB}} + 2\,\gamma_{\langle A\rangle-\{AB\}} + 2\,\gamma_{\langle B\rangle-\{AB\}} \tag{2b}$$

where $D_{AB} = \frac{1}{2}D^A_{AB} + \frac{1}{2}D^B_{AB}$ (cf. Fig. 1). Hence the driving force for interface SSA (ΔG_{iSSA}) can be given as

$$\Delta G_{\mathrm{iSSA}} \equiv G_e - G_i = 2D_{AB}\,\frac{\Delta G^f_{\{AB\}}}{V_{AB}} + 2\,\gamma_{\langle A\rangle-\{AB\}} + 2\,\gamma_{\langle B\rangle-\{AB\}} - 2\,\gamma_{\langle A\rangle-\langle B\rangle}. \tag{3a}$$

If a crystalline solid solution (CSS) is formed at the interface, instead of an amorphous solid solution (SSA), a similar expression for the associated driving force results:

$$\Delta G_{\mathrm{iCSS}} \equiv G_e - G_i = 2D_{AB}\,\frac{\Delta G^f_{\langle AB\rangle}}{V_{AB}} + 2\,\gamma_{\langle A\rangle-\langle AB\rangle} + 2\,\gamma_{\langle B\rangle-\langle AB\rangle} - 2\,\gamma_{\langle A\rangle-\langle B\rangle}. \tag{3b}$$

Next expressions for the energies $\Delta G^f_{\{AB\}}$, $\Delta G^f_{\langle AB\rangle}$, $\gamma_{\langle A\rangle-\langle B\rangle}$, $\gamma_{\langle A\rangle-\langle AB\rangle}$, $\gamma_{\langle A\rangle-\{AB\}}$ and $\gamma_{\langle A\rangle-\{B\}}$, will be derived.

A. Volume Gibbs free energy of formation for the amorphous solid solution ($\Delta G^f_{\{AB\}}$) and for the crystalline solid solution ($\Delta G^f_{\langle AB\rangle}$)

$\Delta G^f_{\{AB\}}$ and $\Delta G^f_{\langle AB\rangle}$ are the net Gibbs free energies needed for the formation of the reactively mixed phases $\{A_cB_{1-c}\}$ and $\langle A_cB_{1-c}\rangle$ from two separated crystalline phases $\langle A\rangle$ and $\langle B\rangle$, where the subscript c has been added to indicate the composition ($c=$mole fraction A). An amorphous phase is thought to be produced from two crystalline elemental phases in two steps: (i) melting of the crystalline phases below the normal melting temperature, assuming that an amorphous phase can be described as an undercooled liquid, and (ii) mixing of the molten phases. Thus, $\Delta G^f_{\{AB\}}$ as a function of composition c and temperature T can be given as

$$\Delta G^{f}_{\{AB\}}(c,T)=G^{\rm melt}(c,T)+G^{\rm mix}(c,T), \tag{4a}$$

where $G^{\rm melt}(c,T)$ is the Gibbs free energy needed to melt the two crystalline phases and $G^{\rm mix}(c,T)$ is the energy needed to mix the two molten phases. For binary (transition) metal-metal systems $G^{\rm melt}(c,T)$ is positive, for $T<T_m$, and for most of these systems $G^{\rm mix}(c,T)$ is negative.

A good estimate of $G^{\rm melt}(c,T)$ is given by (cf. Ref. 12):

$$\begin{aligned} G^{\rm melt}(c,T)&=cG^{\rm melt}_A(T)+(1-c)G^{\rm melt}_B(T)\\ &=cH^{\rm fuse}_A\frac{T^A_m-T}{T^A_m}+(1-c)H^{\rm fuse}_B\frac{T^B_m-T}{T^B_m}, \end{aligned} \tag{4b}$$

where T^A_m and T^B_m are the melt temperatures of the crystalline phases $\langle A\rangle$ and $\langle B\rangle$, respectively, and where it has been assumed that the melting (or fusion) enthalpies, $H^{\rm fuse}_A$ and $H^{\rm fuse}_B$, respectively, are constant in the temperature range considered.

To form a crystalline solid solution, no melting of the crystalline phases is necessary. Thus $\Delta G^{f}_{\langle AB\rangle}$ as a function of c and T is

$$\Delta G^{f}_{\langle AB\rangle}(c,T)=G^{\rm mix}(c,T). \tag{4c}$$

Note that the $G^{\rm mix}$ in Eq. (4c) is different from that in Eq. (4a) [see Eqs. (5a) and (5b)].

The enthalpy of mixing was estimated using the method of Miedema.[11] The entropy of mixing is taken as the configurational entropy. As a result the energy of mixing becomes

$$G^{\rm mix}(c,T)=cF^A_B(c)\Delta H^{\rm interface}_{A\ {\rm in}\ B}-T\Delta S_{\rm conf}, \tag{4d}$$

where $\Delta H^{\rm interface}_{A\ {\rm in}\ B}$ is the enthalpy change upon solution of one mole of A in an infinitely large reservoir of B and $\Delta S_{\rm conf}$ is the change in configurational entropy. $F^A_B(c)$ is the degree to which A atoms are surrounded by B atoms; it is dependent on the degree of order in the system. In liquid solutions and solid solutions, with randomly distributed atoms, this parameter reads

$$F^A_B=C^s_B(c)\equiv\frac{(1-c)V^{2/3}_B}{cV^{2/3}_A+(1-c)V^{2/3}_B} \tag{5a}$$

where $C^s_B(c)$ is the surface fraction of B atoms, i.e., the sum of all surfaces of atoms B divided by the sum of all surfaces of atoms A and B. For amorphous alloys (undercooled liquid solutions) it has been shown that $F^A_B(c)$ can be well estimated by[13]

$$F^A_B(c)=C^S_B[1+5(C^S_AC^S_B)^2] \tag{5b}$$

implying some short-range ordering in the amorphous alloy. For $\Delta S_{\rm conf}$ the expression for the randomly mixed alloy is adopted:

$$\Delta S_{\rm conf}=-R[c\ \ln(c)+(1-c)\ln(1-c)] \tag{5c}$$

although it is realized that the use of this expression is not fully correct if some short-range ordering occurs.

B. Energy of a solid-solid interface

The energy of a grain boundary, i.e., an $\langle A\rangle-\langle A\rangle$ interface, γ^A_{gb}, is taken as $\frac{1}{3}$ of the surface energy, which is an average value for a high angle grain boundary[14,15]

$$\gamma^A_{gb}=\tfrac{1}{3}\gamma_{\langle A\rangle}, \tag{6}$$

where $\gamma_{\langle A\rangle}$ denotes the surface energy of $\langle A\rangle$ (i.e., the energy of an interface between $\langle A\rangle$ and vacuum). An atom in the surface is partially surrounded by vacuum, whereas an atom in the bulk is fully surrounded by other atoms. The surface energy can be attributed to this partial contact with the vacuum. Then, since an evaporated atom is an atom fully in contact with vacuum, the surface energy at $T=0$ K can be estimated by the enthalpy for evaporation of one mole atoms divided by the atomic surfaces of one mole atoms:

$$\gamma^{T=0}_{\langle A\rangle}=\frac{H^{\rm vap}_A}{C_0V^{2/3}_A}, \tag{7a}$$

where C_0 is a constant depending on the shape of the Wigner-Seitz cell of the A atoms and can be taken, on average, as $\approx 4.5\times10^8$ (Ref. 15). An empirical expression for the surface energy, including a temperature dependent entropy effect, is given by[17]

$$\gamma_{\langle A\rangle}(T_1)=\frac{(\gamma_{\langle A\rangle}V^{2/3}_A)^{T=0}+b_AT_1}{(V^{2/3}_A)^{T=T_1}}, \tag{7b}$$

where b_A is a material dependent constant. This expression will be used in the numerical calculations of Secs. VI and VII.

The energy of an interface between a solid phase A and a solid phase B contains two contributions,[15] one is related to the chemical interaction of A and B at the interface and the other is related to the strain due to the mismatch at the interface between the two lattices:

$$\gamma_{\langle A\rangle-\langle B\rangle}=\gamma^{\rm interaction}_{\langle A\rangle-\langle B\rangle}+\gamma^{\rm mismatch}_{\langle A\rangle-\langle B\rangle}. \tag{8a}$$

The interaction energy can be estimated as follows. If the A atoms would be fully surrounded by B atoms, the enthalpy increase would be $\Delta H^{\rm interface}_{A\ {\rm in}\ B}$ per mole $\langle A\rangle$ atoms in an infinitely diluted system [see below Eq. (4d)]. In the interface only a fraction p of the surface of the A atoms in the interface is in contact with B atoms. Thus the enthalpy increase due to the interaction at the interface is taken as $p\Delta H^{\rm interface}_{A\ {\rm in}\ B}$ per mole $\langle A\rangle$ atoms in the interface. In the following, the corresponding contribution of the interaction to the interface energy is equal to this interface enthalpy per unit area which is obtained from the enthalpy increase per mole $\langle A\rangle$ atoms in the interface divided by the area that is occupied by this one mole A atoms in the interface,[15] and thus [cf. Eq. (7a)]

$$\gamma^{\rm interaction}_{\langle A\rangle-\langle B\rangle}=\frac{p\Delta H^{\rm interface}_{A\ {\rm in}\ B}}{pC_0V^{2/3}_A}=\frac{\Delta H^{\rm interface}_{A\ {\rm in}\ B}}{C_0V^{2/3}_A}. \tag{8b}$$

A similar reasoning can be applied with respect to the B atoms in the interface. This leads to the following expression for the contribution to the interface energy due to interaction:

$$\gamma^{\text{interaction}}_{\langle A\rangle-\langle B\rangle}=\frac{\Delta H^{\text{interface}}_{B\ \text{in}\ A}}{C_0 V_B^{2/3}}. \tag{8c}$$

As both expressions [Eqs. (8b) and (8c)] should yield the same result, it follows that

$$\frac{\Delta H^{\text{interface}}_{A\ \text{in}\ B}}{V_A^{2/3}}=\frac{\Delta H^{\text{interface}}_{B\ \text{in}\ A}}{V_B^{2/3}}. \tag{9}$$

According to Ref. 15 the contribution to the interface energy due to mismatch is estimated by

$$\gamma^{\text{mismatch}}_{\langle A\rangle-\langle B\rangle}=\frac{1}{3}\left(\frac{\gamma_{\langle A\rangle}+\gamma_{\langle B\rangle}}{2}\right), \tag{8d}$$

where $\gamma_{\langle A\rangle}$ and $\gamma_{\langle B\rangle}$ denote the surface energies of $\langle A\rangle$ and $\langle B\rangle$ in contact with vacuum, respectively [cf. Eq. (7)].

Thus the energy of an $\langle A\rangle-\langle B\rangle$ interface is given by

$$\begin{aligned}\gamma_{\langle A\rangle-\langle B\rangle}&=\gamma^{\text{mismatch}}_{\langle A\rangle-\langle B\rangle}+\gamma^{\text{interaction}}_{\langle A\rangle-\langle B\rangle}\\&=\frac{1}{3}\left(\frac{\gamma_{\langle A\rangle}+\gamma_{\langle B\rangle}}{2}\right)+\frac{\Delta H^{\text{interface}}_{A\ \text{in}\ B}}{C_0 V_A^{2/3}}.\end{aligned} \tag{8e}$$

Similar to Eq. (8e), the energy of an interface between a solid phase $\langle A\rangle$ and a mixed solid phase $\langle AB\rangle$ can be given as [see also below Eq. (4d)]:

$$\gamma_{\langle A\rangle-\langle B\rangle}=\frac{1}{3}\left(\frac{\gamma_{\langle A\rangle}+\gamma_{\langle AB\rangle}}{2}\right)+\frac{F_B^A\Delta H^{\text{interface}}_{A\ \text{in}\ B}}{C_0 V_A^{2/3}}. \tag{10}$$

An expression for the surface energy of a solid phase $\langle AB\rangle$, $\gamma_{\langle AB\rangle}$, is derived here as follows. If a crystal of A_cB_{1-c} is fractured, a new surface is created. The energy increase of the system can be attributed to the new surface and is the consequence of the bonds broken across the new surface. Initially there are four types of bonds across the surface: *A*-*A*, *B*-*B*, *A*-*B*, and *B*-*A* bonds. The surface fractions of *A* and *B* atoms are, respectively, C_A^s and C_B^s. The fraction of the surface area that is occupied before fracture by a particular bond is given by the product of the surface fractions of the two atoms involved in the kind of bond considered (e.g., the surface fraction of *A*-*A* bonds is $[C_A^s]^2$). After fracture, the atoms of the interface are in contact with vacuum, and their contribution to $\gamma_{\langle AB\rangle}$ corresponds with $\gamma_{\langle A\rangle}$ and $\gamma_{\langle B\rangle}$ for atoms *A* and *B* in the surfaces; breakage of the *A*-*B* and *B*-*A* bonds leads to an additional contribution to the surface energy, equal to

$$-\frac{\Delta H^{\text{interface}}_{A\ \text{in}\ B}}{C_0 V_A^{2/3}}=-\frac{\Delta H^{\text{interface}}_{B\ \text{in}\ A}}{C_0 V_B^{2/3}}$$

[see Eqs. (8b), (8c), and (9)] for *A*-*B* bonds. Hence, realizing that upon fracture, two units of interface area are created from one unit area of the section along which fracture proceeded, it follows for $\gamma_{\langle AB\rangle}$ that

$$\begin{aligned}2\gamma_{\langle AB\rangle}=&\,2\gamma_{\langle A\rangle}(C_A^s)^2+2\gamma_{\langle B\rangle}(C_B^s)^2+2C_A^sC_B^s\\&\times\left(\gamma_{\langle A\rangle}+\gamma_{\langle B\rangle}-\frac{\Delta H^{\text{interface}}_{A\ \text{in}\ B}}{C_0 V_A^{2/3}}-\frac{\Delta H^{\text{interface}}_{B\ \text{in}\ A}}{C_0 V_B^{2/3}}\right)\end{aligned} \tag{11a}$$

which, using Eq. (9), becomes

$$\gamma_{\langle AB\rangle}=C_A^s\gamma_{\langle A\rangle}+C_B^s\gamma_{\langle B\rangle}-C_A^sC_B^s\,\frac{\Delta H^{\text{interface}}_{A\ \text{in}\ B}}{C_0 V_A^{2/3}}. \tag{11b}$$

The first two terms at the right-hand side of Eq. (11a) comprise the energy contribution of the $\langle A\rangle$-vacuum and $\langle B\rangle$-vacuum interfaces resulting from *A*-*A* and *B*-*B* bonds in the original crystal. The last terms provide the energy contribution of $\langle A\rangle$-vacuum and $\langle B\rangle$-vacuum interfaces resulting from *A*-*B* and *B*-*A* bonds in the original crystal, thereby taking into account the loss of interaction of these *A* and *B* atoms.

C. Energy of a solid-amorphous or solid-liquid interface

Establishing contact between an infinitely large body of a crystalline phase, with only $\langle A\rangle$-$\langle A\rangle$ bonds, and an infinitely large body of an amorphous or liquid phase, with only $\{A\}$-$\{A\}$ bonds, creates an interface across which $\langle A\rangle$-$\{A\}$ bonds occur. This is associated with an energy increase of the system which is defined as the interface energy. The interface energy consists of an enthalpy contribution and an entropy contribution. It will be assumed that the enthalpy contribution arises from the solid phase at the interface and that the entropy contribution arises from the liquid or amorphous phase at the interface.[15,16]

The enthalpy of the interface is associated with the newly formed $\langle A\rangle$-$\{A\}$ bonds. Assuming that the $\langle A\rangle$-$\{A\}$ bonding is rather a liquid bonding than a crystal bonding,[16] the enthalpy of the interface scales with H_A^{fuse}. The scaling factor *p* is assumed to be the fraction of the surface of the atom $\langle A\rangle$ at the interface that makes contact with the amorphous phase $\{A\}$ at the interface.[15] The interface enthalpy is thus estimated by pH_A^{fuse} per mole atoms $\langle A\rangle$ at the interface. The interface enthalpy per unit area is the energy per mole $\langle A\rangle$ atoms in the interface divided by the area that is occupied by this one mole $\langle A\rangle$ atoms in the interface[15] [cf. Eq. (8b)], i.e.,

$$\gamma^{\text{enthalpy}}_{\langle A\rangle\text{-}\{A\}}=\frac{pH_A^{\text{fuse}}}{pC_0V_A^{2/3}}=\frac{H_A^{\text{fuse}}}{C_0V_A^{2/3}}. \tag{12a}$$

The entropy contribution to the interface energy can be estimated using a structural model for the $\langle A\rangle$-$\{A\}$ interface constructed by Spaepen *et al.*[17] Assuming that the vibrational entropy does not change in the crystalline phase nor in the liquid phase by introducing an interface, only the change of configurational entropy upon interface creation has to be considered. It is assumed that the configurational entropy of the solid does not change (see above). At the interface the configurational entropy of the liquid is lowered (by the ordering effect due to the nearby crystalline solid). This corresponds with an energy increase: the entropy contribution to the interface energy. Only the first two atomic layers of the liquid phase at the interface have a configurational entropy significantly lower than that of the bulk liquid phase. This difference in entropy is calculated to be $0.904k$ (k = Boltzmann's constant) per atom of the first layer of the liquid phase at the interface.[17] As there is $\frac{3}{4}$ atom of the liquid phase at the interface per atom of the solid phase at the interface,[17] the entropy difference per mole atoms of the

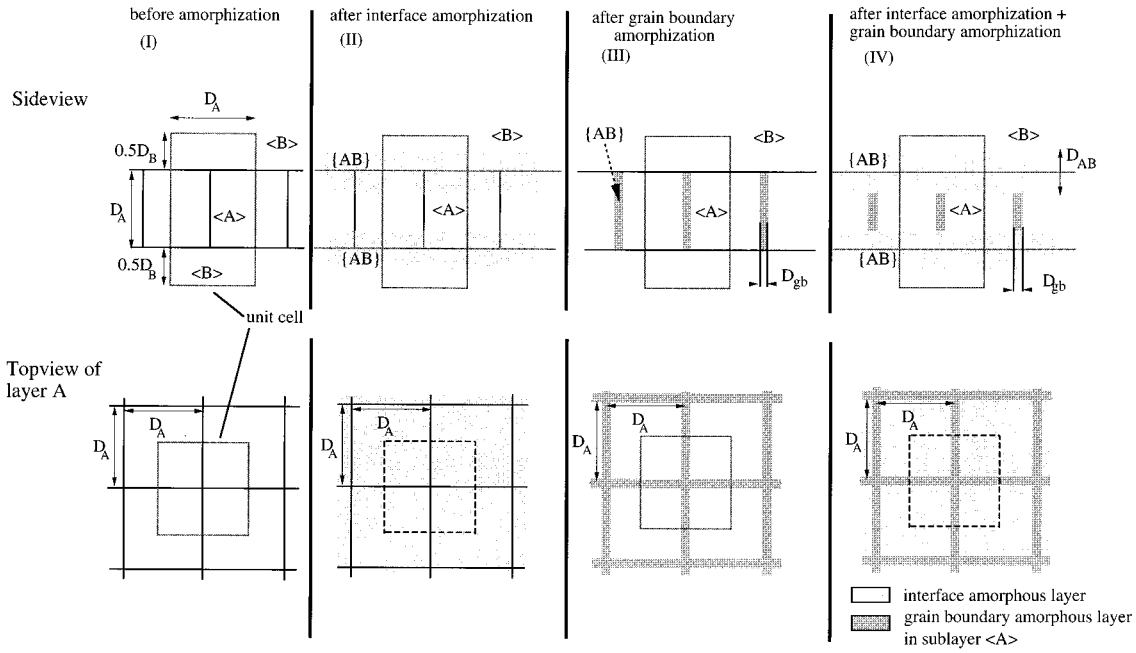

FIG. 2. Schematic drawing of an A-B multilayer with grain boundaries in the A sublayer perpendicular to the interface before and after amorphization. (I): the initial situation. (II): the situation after amorphization only at the A/B interface. (III): the situation after only grain-boundary amorphization in $\langle A\rangle$. (IV): the situation after both A/B interface and grain-boundary amorphization in $\langle A\rangle$. D_A and D_B are the initial thicknesses of the crystalline phases $\langle A\rangle$ and $\langle B\rangle$. D_{AB} and D_{gb} are the thicknesses of the amorphous phases along the interface and along the grain boundary, respectively. The thermodynamics of interface amorphization are calculated for a unit cell of lateral area of 10×10 nm^2 and with a height equal to the sum of D_A ($=10$ nm) and D_B ($=10$ nm).

solid phase at the interface becomes: $\frac{3}{4}\times0.904k\times N_A=0.678R$ in J K^{-1} mol^{-1}, where N_A=Avogadro's number and $R=N_Ak$ is the gas constant. Thus the entropy contribution to the interface energy per unit area interface [see above Eq. (12a)], with $p=\frac{1}{3}$ (Ref. 15) is

$$\gamma^{\text{entropy}}_{\langle A\rangle\text{-}\{A\}}=\frac{0.678R}{pC_0V_A^{2/3}}\,T=\frac{1.9RT}{C_0V_A^{2/3}}. \tag{12b}$$

Thus the interface energy as obtained by summing Eqs. (12a) and (12b) becomes

$$\gamma_{\langle A\rangle\text{-}\{A\}}=\gamma^{\text{enthalpy}}_{\langle A\rangle\text{-}\{A\}}+\gamma^{\text{entropy}}_{\langle A\rangle\text{-}\{A\}}=\frac{H_A^{\text{fuse}}+1.9RT}{C_0V_A^{2/3}}. \tag{12c}$$

Now considering an $\langle A\rangle$-$\{AB\}$ interface, three contributions to the interface energy can be recognized:[11,15]

$$\gamma_{\langle A\rangle\text{-}\{AB\}}=\gamma^{\text{enthalpy}}_{\langle A\rangle\text{-}\{AB\}}+\gamma^{\text{entropy}}_{\langle A\rangle\text{-}\{AB\}}+\gamma^{\text{interaction}}_{\langle A\rangle\text{-}\{AB\}}. \tag{13a}$$

The enthalpy contribution to the interface energy arises from the solid phase $\langle A\rangle$ at the interface and is estimated according to Eq. (12a). The entropy contribution to the interface energy arises from the liquid phase $\{AB\}$ at the interface and is taken according to Eq. (12b), with the substitution of V_A by V_{AB}. The interaction energy of $\langle A\rangle$-$\{AB\}$ is [cf. Eq. (10)]

$$\gamma^{\text{interaction}}_{\langle A\rangle\text{-}\{AB\}}=\frac{F_B^A\Delta H^{\text{interface}}_{A\text{ in }B}}{C_0V_A^{2/3}}. \tag{13b}$$

Thus the interface energy of an $\langle A\rangle$-$\{AB\}$ interface becomes

$$\gamma_{\langle A\rangle\text{-}\{AB\}}=\frac{H_A^{\text{fuse}}+F_B^A\Delta H^{\text{interface}}_{A\text{ in }B}}{C_0V_A^{2/3}}+\frac{1.9RT}{C_0V_{AB}^{2/3}}. \tag{13c}$$

III. SOLID-STATE AMORPHIZATION AT GRAIN BOUNDARIES

The sublayers of a crystalline multilayer normally consist of small crystals with lateral dimensions of the same order as the layer thickness. Consequently, in such a thin layer a lot of grain boundaries perpendicular to the interface exist. A schematic drawing of a binary A-B multilayer before and after occurrence of both interface and grain-boundary amorphization in the A sublayer is given in Fig. 2. Four situations are sketched: (I) the initial situation, before SSA has occurred; (II) after only interface SSA; (III) after only grain-boundary SSA, and (IV) after both interface SSA and grain-boundary SSA.

The thermodynamics of SSA will be described for cases II, III, and IV for a unit cell of volume $D_AD_A(D_A+D_B)$, as defined in Fig. 2; the grains in layer $\langle A\rangle$ are taken as cubes with edges D_A (D_A and D_B are the initial layer thicknesses of $\langle A\rangle$ and $\langle B\rangle$, respectively). Because SSA along grain boundaries in $\langle B\rangle$ is taken not to occur and the presence of grain boundaries has little influence on interface SSA [as will be shown in Sec. V; see, for example Fig. 3(c) versus Fig. 3(d)], the energy effect of grain boundaries in $\langle B\rangle$ can be ignored in the following treatment.

The total Gibbs free energy of the unit cell before amorphization (situation I in Fig. 2), G_i, is given by [cf. Eq. (1)]

$$G_i={D_A}^3\frac{G_{\langle A\rangle}}{V_A}+{D_A}^2D_B\frac{G_{\langle B\rangle}}{V_B}+2\gamma_{\langle A\rangle\text{-}\langle B\rangle}{D_A}^2+2\gamma^A_{gb}{D_A}^2. \tag{14}$$

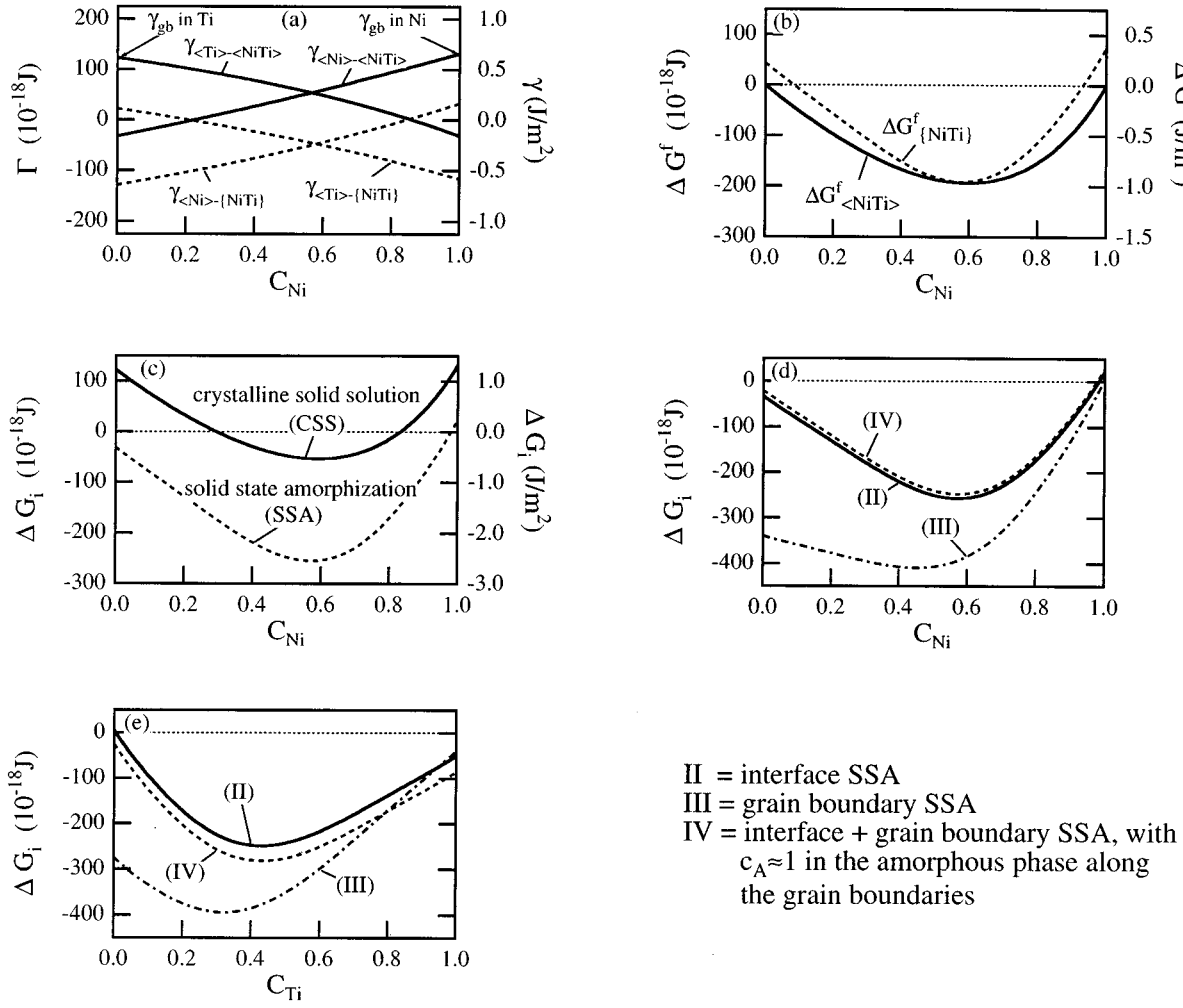

FIG. 3. Results of the thermodynamic model for solid-state amorphization (SSA) in the Ni-Ti system at 525 K for a unit cell of lateral area of 10×10 nm^2 and with a height equal to the sum of D_A (=10 nm) and D_B (=10 nm) (see Figs. 1 and 2). (a) The interface energies as a function of the Ni concentration in the amorphous phase. The ordinate on the left-hand side gives the total energy of an interface in the unit cell; the ordinate on the right-hand side gives the interface energy per unit area. (b) The Gibbs free energy of formation of the amorphous phase at the interface and of the corresponding crystalline solid solution, as given by Eqs. (4a) and (4c). (c) The negative of the driving force (ΔG_i) for the formation and one atom thick amorphous layer (D_{AB}=2.1 Å) and the formation of a one atom thick crystalline solid solution layer at the interface. (d) The negative of the driving force (ΔG_i) for amorphization occurring in the three situations depicted in Fig. 2: (II) only interface amorphization, as a function of the Ni concentration in the amorphous phase at the interface; (III) only grain-boundary amorphization in the Ni layer, as a function of the Ni concentration in the amorphous phase at the grain-boundary; (IV) both interface and grain-boundary amorphization, as a function of the Ni concentration in the amorphous phase at the interface. In situation (IV) the Ni concentration in the amorphous phase at the grain boundary is ≈1. (e) similar to (d) but now applied to SSA in the Ti layer.

The total Gibbs free energy of the unit cell after interface amorphization (situation II in Fig. 2), G_e^{II} reads, [cf. Eq. (2)]

$$G_e^{II} = {D_A}^3 \frac{G_{\langle A\rangle}}{V_A} + {D_A}^2 D_B \frac{G_{\langle B\rangle}}{V_B} + 2D_{AB}^A {D_A}^2 \frac{G^f_{\{AB\}}}{V_{AB}} + 2{D_A}^2 \gamma_{\langle A\rangle\text{-}\{AB\}} + 2{D_A}^2 \gamma_{\langle B\rangle\text{-}\{AB\}} + 2(D_A - D_{AB}^A) D_A \gamma_{gb}^A, \quad (15)$$

where D_{AB}^A is the thickness of the amorphous layer grown in the original layer A (cf. Fig. 1). The total Gibbs free energy of the unit cell after only grain-boundary amorphization (situation III in Fig. 2), G_e^{III}, is given by

$$G_e^{III} = {D_A}^3 \frac{G_{\langle A\rangle}}{V_A} + {D_A}^2 D_B \frac{G_{\langle B\rangle}}{V_B} + 2D_A D_{gb}(D_A - \tfrac{1}{2}D_{gb}) \times \frac{G^f_{\{AB\}}}{V_{AB}} + 2(D_A - D_{gb})^2 \gamma_{\langle A\rangle\text{-}\langle B\rangle} + 2[2D_{gb}(D_A - D_{gb})]\gamma_{\langle B\rangle\text{-}\{AB\}} + 4D_A(D_A - D_{gb})\gamma_{\langle A\rangle\text{-}\{AB\}}, \quad (16)$$

where D_{gb} is the layer thickness of the amorphous phase at the grain boundary in layer A (Fig. 2). The total Gibbs free energy of the unit cell after both interface SSA and grain-boundary SSA (situation IV in Fig. 2), G_e^{IV}, is given by

$$G_e^{IV}=D_A{}^3\frac{G_{\langle A\rangle}}{V_A}+D_A{}^2D_B\frac{G_{\langle B\rangle}}{V_B}+2D_{AB}D_A{}^2\frac{G^f_{\{AB\}i}}{V_{AB}}+(2D_A-D_{gb})(D_A-D^A_{AB})D_{gb}\frac{G^f_{\{AB\}gb}}{V_{AB}}+2(D_A-D_{gb})^2\gamma_{\langle A\rangle\text{-}\{AB\}i}+4(D_A-D_{gb})\times(D_A-D^A_{AB})\gamma_{\langle A\rangle\text{-}\{AB\}gb}+2D_A{}^2\gamma_{\langle B\rangle\text{-}\{AB\}i}, \quad (17)$$

where the subscript i refers to the amorphous phase at the interface and the subscript gb refers to the amorphous phase at the grain boundary in layer A.

The thermodynamic model given in Secs. II and III applies to initially crystalline binary (metal) systems. Considerations of two phase A-B systems where initially one phase is crystalline ($\langle A\rangle$) and one phase is amorphous ($\{B\}$), can be of interest (see Sec. VI). By changing the subscript $\langle B\rangle$ in Eqs. (1)–(3) and (14)–(17) into the subscript $\{B\}$, the model given describes a crystalline-amorphous binary system as well. Then the only energy term for which no expression has been derived yet, is the interface energy $\gamma_{\{B\}\text{-}\{AB\}}$. An estimation can be made with reference to the discussion in Sec. II, on the interface energy $\gamma_{\langle A\rangle\text{-}\{AB\}}$. The enthalpy and entropy contributions considered there are obviously nil for the case considered here. Hence the interface energy $\gamma_{\{B\}\text{-}\{AB\}}$ is only due to chemical to interaction:

$$\gamma_{\{B\}\text{-}\{AB\}}=F^B_A\frac{\Delta H^{\text{interfcace}}_{B\ \text{in}\ A}}{C_0V_B^{2/3}}=F^B_A\frac{\Delta H^{\text{interfcace}}_{A\ \text{in}\ B}}{C_0V_A^{2/3}}, \quad (18)$$

where Eq. (9) has been applied. Further as the initial B layer is amorphous instead of crystalline, the Gibbs free energy of formation ($\Delta G^f_{\{AB\}}$) as given in Eqs. (4a)–(4d) has to be changed. This is achieved by taking $H_B^{\text{fuse}}=0$ in Eq. (4b).

IV. COMPARISON OF SURFACE AND INTERFACE ENERGIES OF CRYSTALLINE AND AMORPHOUS PHASES; MAXIMUM THICKNESS OF THE AMORPHOUS LAYER

A. Surface and interface energies

Clearly the interface energies play an important role in the competition between the formations of a crystalline solid solution and an amorphous solid solution [see Eqs. (3), (14)–(17)]. If a crystalline solid solution is formed, two crystalline-crystalline interfaces, i.e., $\langle A\rangle$-$\langle AB\rangle$ and $\langle B\rangle$-$\langle AB\rangle$, are created. If an amorphous phase is formed, two crystalline-amorphous interfaces are created, i.e., $\langle A\rangle$-$\{AB\}$ and $\langle B\rangle$-$\{AB\}$. It will be shown below that in general the crystalline-amorphous interface is energetically more favorable. First the surface energies of the corresponding crystalline and amorphous phases are compared. Next the parent $\langle A\rangle$-product ($\langle AB\rangle$ or $\{AB\}$) interface energies will be compared.

The surface enthalpy of the crystalline phase can be expressed by Eq. (7a). Analogously, the surface enthalpy of the liquid (amorphous) phase can be expressed by

$$\gamma^{T=0}_{\{A\}}=\frac{H_A^{\text{vap}}-H_A^{\text{fuse}}}{C_0V_A^{2/3}}. \quad (19)$$

A comparison of Eqs. (7a) and (19) shows that of course the surface enthalpy of an amorphous phase is lower than the surface enthalpy of a crystalline phase. According to Ref. 15, the entropy contributions to the surface energy are about equal for the crystalline phase and the amorphous phase:

$$\gamma^{\text{entropy}}_{\langle A\rangle}\approx\gamma^{\text{entropy}}_{\{A\}}=-\frac{RT}{C_0V_A^{2/3}}. \quad (20)$$

Hence, the surface energy of an amorphous phase is lower than the surface energy of a crystalline phase. Obviously the bulk Gibbs free energy of the amorphous phase, below T_{melt}, is larger than the bulk Gibbs free energy of the crystalline phase. It can be concluded that a thin, free standing amorphous layer can be more stable than the corresponding crystalline layer as long as the difference between the bulk Gibbs free energies of the amorphous and crystalline layers is smaller than the negative of the difference between the surface energies of the amorphous and crystalline layers.

The energy of a crystalline-crystalline interface is given by Eq. (10) and the energy of a crystalline-amorphous interface is given by Eq. (13c). Since the interaction-energy terms in Eqs. (10) and (13c) are the same, they can be ignored in a comparison of the interface energies concerned. Thus two expressions for correspondingly reduced interface energies can be defined (denoted by an asterisk). Additionally using Eq. (11b) it then follows from Eq. (10) for the crystalline-crystalline interface:

$$\gamma^*_{\langle A\rangle\text{-}\langle AB\rangle}=\frac{1}{6}\left(\gamma_{\langle A\rangle}+C^s_A\gamma_{\langle A\rangle}+C^s_B\gamma_{\langle B\rangle}-C^s_AC^s_B\frac{\Delta H^{\text{interface}}_{A\ \text{in}\ B}}{C_0V_A^{2/3}}\right) \quad (21)$$

and from Eq. (13c) it follows directly

$$\gamma^*_{\langle A\rangle\text{-}\{AB\}}=\frac{H_A^{\text{fuse}}}{C_0V_A^{2/3}}+\frac{1.9RT}{C_0V_{AB}^{2/3}}. \quad (22)$$

A lower limit for $\gamma^*_{\langle A\rangle\text{-}\langle AB\rangle}$ can be obtained as follows. The fourth term on the right-hand side of Eq. (21) is, for all systems in which SSA occurs, positive and small as compared to the sum of the other three terms. Therefore, it holds for a lower limit for $\gamma^*_{\langle A\rangle\text{-}\langle AB\rangle}$ [using Eq. (7a) for $\gamma_{\langle A\rangle}$ and a similar expression for $\gamma_{\langle B\rangle}$]:

$$\gamma^{*,\ \text{lower limit}}_{\langle A\rangle\text{-}\langle AB\rangle}=\tfrac{1}{6}(\gamma_{\langle A\rangle}+C^s_A\gamma_{\langle A\rangle}+C^s_B\gamma_{\langle B\rangle})=\frac{1}{6}\left(\frac{H_A^{\text{vap}}}{C_0V_A^{2/3}}+C^s_A\frac{H_A^{\text{vap}}}{C_0V_A^{2/3}}+C^s_B\frac{H_B^{\text{vap}}}{C_0V_B^{2/3}}\right). \quad (23)$$

Recognizing that $H^{\text{fuse}}<\frac{1}{12}H^{\text{vap}}$ (Ref. 14), it follows from Eq. (23) that a lower limit for $\gamma_{\langle A\rangle\text{-}\langle AB\rangle}$ can be assessed from

$$\gamma^{*,\ \text{lower limit}}_{\langle A\rangle\text{-}\langle AB\rangle} = \frac{2H_A^{\text{fuse}}}{C_0 V_A^{2/3}} + C_A^s \frac{2H_A^{\text{fuse}}}{C_0 V_A^{2/3}} + C_B^s \frac{2H_B^{\text{fuse}}}{C_0 V_B^{2/3}}. \quad (24)$$

As all known SSA processes take place below 800 K, the second term on the right-hand side of Eq. (22) is smaller than or at most of the same order as the first term on the right-hand side of Eq. (22) (for A=La this is only true below 600 K). Therefore an upper limit for $\gamma^*_{\langle A\rangle\text{-}\{AB\}}$ can be assessed from

$$\gamma^{*,\ \text{upper limit}}_{\langle A\rangle\text{-}\{AB\}} = \frac{2H_A^{\text{fuse}}}{C_0 V_A^{2/3}}. \quad (25)$$

From Eqs. (24) and (25) it can be concluded that the upper limit for $\gamma^*_{\langle A\rangle\text{-}\{AB\}}$ is always smaller than the lower limit for $\gamma^*_{\langle A\rangle\text{-}\langle AB\rangle}$. Hence, the crystalline-amorphous interface has a lower energy than the crystalline-crystalline interface. Therefore, it can be concluded that also a product amorphous layer sandwiched between parent crystalline layers can be more stable than the corresponding crystalline layer, as long as the difference between the bulk Gibbs free energies of the amorphous and the corresponding crystalline product layer is smaller than the negative of the difference between the energies of the amorphous-crystalline interface and the crystalline-crystalline interface.

It should be realized that the discussion in this section implies that an amorphous solid solution, instead of a crystalline solid-solution product layer develops because it is more stable thermodynamically, rather than that a kinetic condition (Ref. 1) is invoked to explain the occurrence of an amorphous phase.

B. Maximum thickness of the amorphous phase

The treatment above directly suggests the calculation of a maximum thickness for an amorphous layer. It follows straightforwardly for the maximum thickness $D_{AB}^{\max}$ of an amorphous product layer $\{AB\}$ between crystalline parent layers:

$$D_{AB}^{\max} = \frac{\Sigma \text{ interface energies for crystalline product layer} - \Sigma \text{ interface energies for amorphous product layer}}{\dfrac{G_{\{AB\}} - G_{\langle AB\rangle}}{V_{AB}}} \quad (26)$$

In the special case of a pure, free standing metal layer, Eq. (26) reduces to a simple expression for $D_A^{\max}$ (in vacuum). The difference between the surface energies involved is according to Eqs. (7a), (19), and (20)

$$\Sigma(\text{surface energy of } \langle A\rangle) - \Sigma(\text{surface energy of } \{A\}) = 2(\gamma_{\langle A\rangle} - \gamma_{\{A\}}) = 2\frac{H_A^{\text{fuse}}}{C_0 V_A^{2/3}}. \quad (27)$$

Substituting Eq. (27) in Eq. (26) and taking $H_A^{\text{fuse}}[(T_m^A - T)/T_m^A]$ for $G_{\{A\}} - G_{\langle A\rangle}$ [cf. Eq. (4b)], gives

$$D_A^{\max}(\text{in vacuum}) = \frac{2H_A^{\text{fuse}}/C_0 V_A^{2/3}}{(G_{\{A\}} - G_{\langle A\rangle})/V_A} = \frac{2H_A^{\text{fuse}}/C_0 V_A^{2/3}}{H_A^{\text{fuse}}[(T_m^A - T)/T_m^A]/V_A} = \frac{2V_A^{1/3}}{C_0}\frac{T_m^A}{T_m^A - T}. \quad (28)$$

A case of larger interest for practice involves the analogous calculation of the maximum thickness of an amorphous

TABLE I. Values of parameters used in the calculations. V_A is the molar volume of pure crystalline solid A (Ref. 14); H_A^{fuse} is the enthalpy of fusion (Ref. 14); $\Delta H_{A \text{ in } B}^{\text{interface}}$ is the enthalpy change upon solution of one mole A in an infinitive large reservoir of B (Ref. 14); T_m^A is the melting temperature of A (Ref. 14) and b_A is a factor reflecting entropy change as defined in Eq. (7b) (Ref. 15).

Parameter→ ↓ element A	V_A (10^{-6} m^3)	H_A^{fuse} (kJ/mol)	$\Delta H_{A \text{ in } B}^{\text{interface}}$ (kJ/mol)	T_m^A (K)	$(\gamma V_A^{2/3})^{T=0}$ (10^{-3} J/mol)	b_A (10^{-7} J/K)
Ni	6.6	17.48	A=Ni, B=Ti −126	1726	0.75	−0.47
Ti	10.6	15.45	A=Ti, B=Ni −154	1943	0.92	−0.73
Zr	14.0	21.00	A=Zr, B=Ni −237	2125	1.05	−0.47
Cu	7.1	13.05	A=Cu, B=Y −70	1358	0.61	−0.44
Y	19.9	11.40	A=Y, B=Cu −117	1799	0.71	−0.71

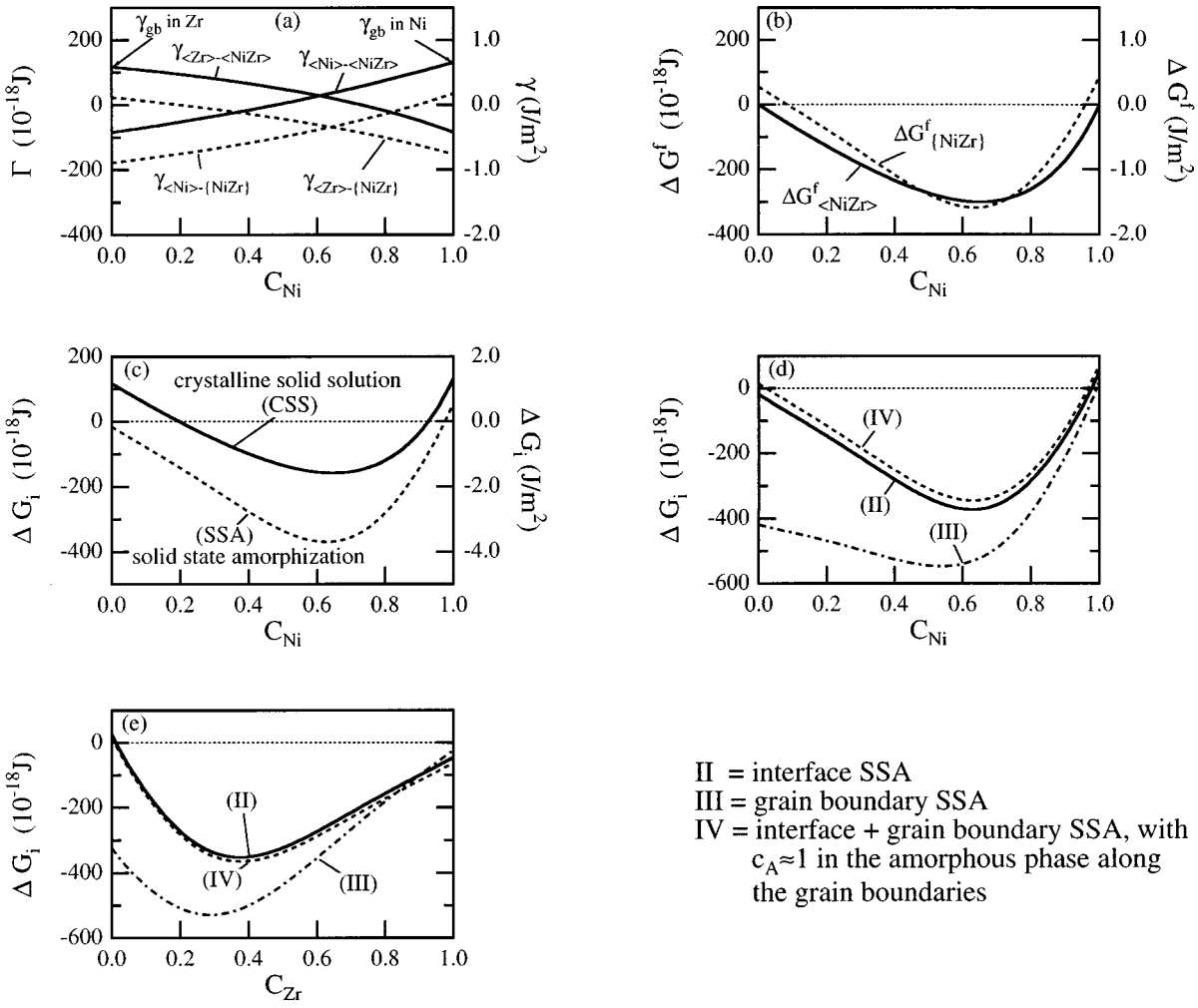

FIG. 4. Results of the thermodynamic model for solid-state amorphization (SSA) in the Ni-Zr system at 575 K. For details, see caption of Fig. 3.

layer $\{A\}$ on a crystalline substrate $\langle A\rangle$. Assuming that a high angle grain boundary occurs between the corresponding crystalline layer $\langle A\rangle$ and the substrate $\langle A\rangle$, substitution of Eqs. (6), (7a), (2c), (19), and (20) in Eq. (26) leads to

$$D_A^{\max}=\frac{(\gamma_{\langle A\rangle}+\gamma_{gb}^A)-(\gamma_{\{A\}}+\gamma_{\langle A\rangle-\{A\}})}{(G_{\{A\}}-G_{\langle A\rangle})/V_A}$$

$$=\frac{V_A^{1/3}}{C_0}\frac{T_m^A}{T_m^A-T}\frac{\frac{1}{3}H_A^{\mathrm{vap}}-2\frac{1}{3}RT}{H_A^{\mathrm{fuse}}}. \tag{29}$$

Recognizing that $2\frac{1}{3}RT \ll \frac{1}{3}H_A^{\mathrm{vap}}$ this becomes

$$D_A^{\max}\approx\frac{2V_A^{1/3}}{C_0}\frac{T_m^A}{T_m^A-T}\frac{H_A^{\mathrm{vap}}}{6H_A^{\mathrm{fuse}}}=D_A^{\max}(\text{in vacuum})\,\frac{H_A^{\mathrm{vap}}}{6H_A^{\mathrm{fuse}}}. \tag{30}$$

V. APPLICATION TO CRYSTALLINE-CRYSTALLINE BINARY SYSTEMS

The model presented in Secs. II and III will be used to investigate the possible occurrence of interface and/or grain boundary SSA and crystalline solid solution (CSS) formation in binary crystalline-crystalline systems for which corresponding data have been reported in the literature. The energy contributions essential for a thermodynamic description are calculated as a function of the composition of the amorphous (or crystalline solid-solution) phase using the parameters given in Table I, for a unit cell of lateral area of 10×10 nm^2 and with a height equal to the sum of D_A (=10 nm) and D_B (=10 nm) (see Figs. 1 and 2). The product layer (SSA or CSS) is taken as 1 atom thick (defined as the interplanar spacing of the closed packed planes), representing the initial stage of the transformation. For each system considered, the temperature used in the calculations was taken as that of the heat treatment as applied in the corresponding experiments reported in the literature. The zero values of ΔG^f are defined with respect to a mechanical mixture of $\langle A\rangle$ and $\langle B\rangle$.

The driving forces are defined as the negative of the difference between the energy of the unit cell after reaction and the energy of the unit cell before reaction. (Thus, in a system without grain boundaries the driving forces are $-\Delta G_{\mathrm{iSSA}}$ [Eq. (3a)] and $-\Delta G_{\mathrm{iCSS}}$ [Eq. (3b)] for interface SSA and CSS, respectively. In a system with grain boundaries the driving force for SSA is (Fig. 2): $-\Delta G_i=G_i-G_e$ using Eqs. (15)–(17) and Eq. (14)).

TABLE II. Comparison between experimental observations and predictions of the model.

System	Ref.	Experimental observations	Predictions
Ni-Ti	3, 4	at $T=525$ K	at $T=525$ K
		- interface SSA	- interface SSA
		- grain boundary SSA in Ti	- grain boundary SSA in Ti
		- no grain boundary SSA in Ni	- no grain boundary SSA in Ni
Ni-Zr	5, 18, 19	at $T=575$ K	at $T=575$ K
		- interface SSA	- interface SSA
		- grain boundary SSA in Zr	- grain boundary SSA in Zr
		- no grain boundary SSA in Ni	- no grain boundary SSA in Ni
Cu-Y	6	at $T=300$ K	at $T=300$ K
		- interface SSA	- interface SSA
		- grain boundary SSA in Y	- grain boundary SSA in Y
		- no grain boundary SSA in Cu	- no grian boundary SSA in Cu

Because the initial stage of SSA is studied, in the case of both interface and grain boundary SSA (situation IV in Fig. 2) the composition of the amorphous phase at the grain boundary is taken different from that at the interface: i.e., the amorphous phase at the grain boundary in A has a composition of $c_A=1$, whereas the A content of the amorphous phase at the interface ranges from 0 to 1. To illustrate the concentration dependency of the driving force for grain boundary amorphization, the driving force for only grain boundary SSA is also given separately as a function of the composition of the amorphous phase along the grain boundaries [situation III in Fig. 2(a)].

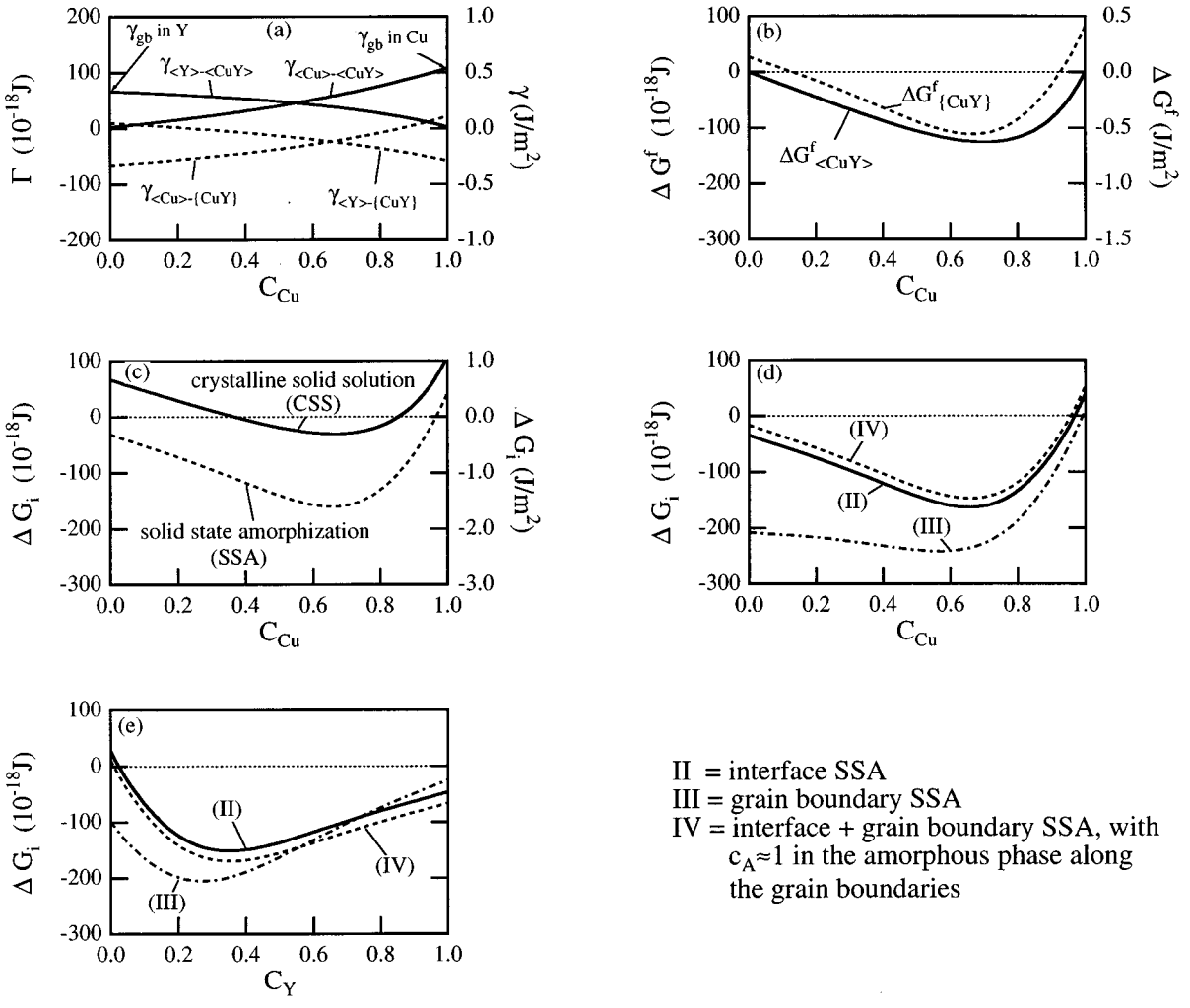

FIG. 5. Results of the thermodynamic model for solid-state amorphization (SSA) in the Cu-Y system at 300 K. For details, see caption of Fig. 3.

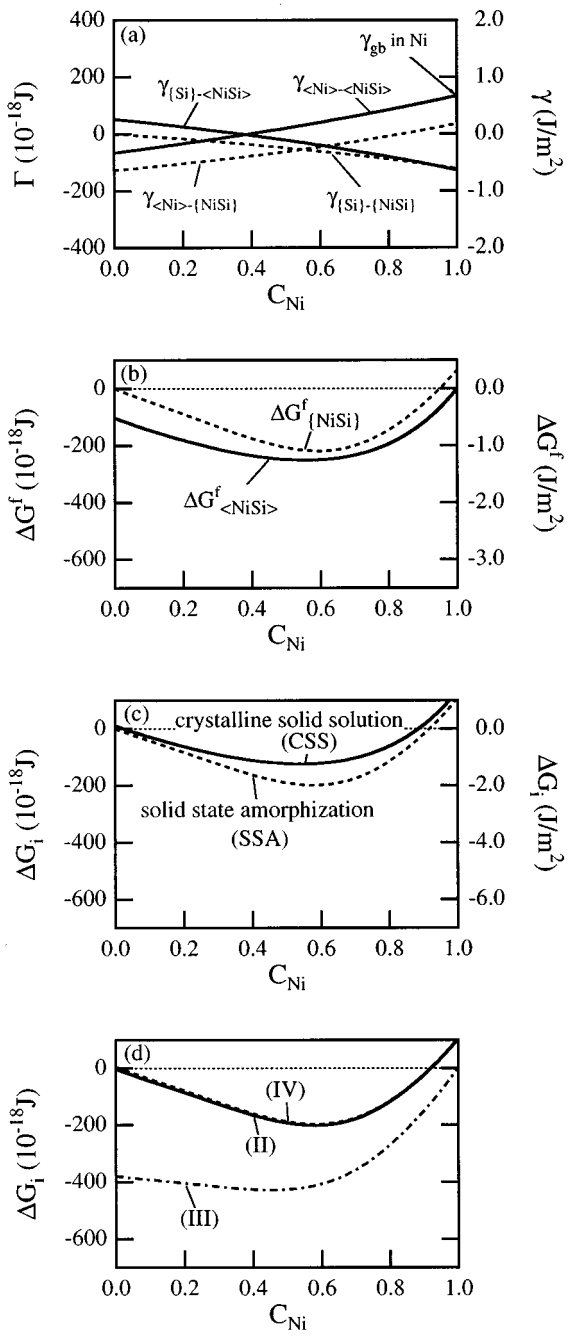

FIG. 6. Results of the thermodynamic model for solid state amorphization (SSA) in the Ni-*a*Si system at 675 K. For details, see caption of Fig. 3.

A. Ni-Ti system

Results of the thermodynamic calculations for the formation of SSA and of CSS in a Ni-Ti system are depicted in Figs. 3(a)–3(c). The interface energies of the Ni-Ti system are given in Fig. 3(a), where Γ denotes the interface energy per unit cell as defined above. The Gibbs free energy of formation of a SSA layer [Eq. (4a)] and of a CSS layer [Eq. (4c)] are given in Fig. 3(b). The total driving forces for the formation at the interface of an one atom thick layer of both an amorphous phase [Eq. (3a)] and a crystalline solid solution [Eq. (3b)] are given in Fig. 3(c) as a function of the Ni content of the product phase.

It follows from Fig. 3(c) that there is always a driving force for amorphization except for an amorphous phase of high Ni content. The formation of a CSS layer has only a (relatively small) driving force within a range of Ni content from about 0.3 to 0.8. Clearly, in this concentration range the driving force for SSA at the interface is larger than that for the formation of the corresponding CSS at the interface. Although the Gibbs free energy of formation of the amorphous phase [Eq. (4a), curved dashed line in Fig. 3(b)] is less negative than the Gibbs free energy of formation of a solid solution [Eq. (4c), full line in Fig. 3(b)], the formation of an amorphous phase is favored by the creation of amorphous-crystalline interfaces with energies smaller than those of the corresponding crystalline-crystalline interfaces [Fig. (3a)]. Hence, the model predicts interface solid state amorphization in a Ni-Ti system.

The driving forces ($=-\Delta G_i$) for the formation of an amorphous phase along the interface and/or along the grain boundaries in a sublayer (see the three cases II–IV considered in Sec. III and indicated in Fig. 2) are given in Fig. 3(d) for SSA along grain boundaries in the Ni layer, and in Fig. 3(e) for SSA along grain boundaries in the Ti layer. Again, only the initial stages of interface and/or of the grain boundary amorphization have been considered, i.e., the calculations pertain to a product layer of one atom thickness. Thus, also the composition of the amorphous phase at the grain boundaries is taken different from that at the interface: the (initial) amorphous phase at the Ni (Ti) grain boundary has a Ni (Ti) content of $c_{Ni} \cong 1$ ($c_{Ti} \cong 1$) whereas the Ni (Ti) content of the amorphous phase at the interface is considered for $0 \leqslant C_{Ni}$ [$C_{Ti} \leqslant 1$, i.e., the abscissa value in Figs. 3(d) and 3(e)].

There is no driving force for the initial situation of only grain boundary SSA in the Ni layer: see curve III in Fig. 3(d) [obtained using Eq. (16)] for a Ni rich amorphous phase at the grain boundary. Hence, a nucleation barrier exists for grain boundary SSA in the Ni layer. Consequently the driving force for only interface SSA [curve II in Fig. 3(d)] is larger than that for simultaneous interface and grain boundary SSA in the Ni layer [curve IV in Fig. 3(d)]. Therefore, only interface SSA is predicted in the Ni layer.

On the other hand, there is a driving force for the initial situation of only grain boundary SSA in the Ti layer [curve III in Fig. 3(e)]. Hence, no nucleation barrier exists for gain boundary SSA in the Ti layer. Consequently, the driving force for only interface SSA [curve II in Fig. 3(e)] is smaller than the driving force for simultaneous interface and grain boundary SSA in the Ti layer [curve IV in Fig. 3(e)].

In the calculations high angle grain boundaries have been considered [cf. Eq. (6)]. If it is assumed that the energy of high angle grain boundaries is a maximum for grain bound-

TABLE III. Values of parameters used in the calculations. V_A is the molar volume of pure crystalline (or amorphous) solid A (Ref. 14); H_A^{fuse} is the enthalpy of fusion (Ref. 14); $\Delta H_{A \text{ in } B}^{\text{interface}}$ is the enthalpy change upon solution of one mole A in an infinitive large reservoir of B (Ref. 14); T_m^A is the melting temperature of A (Ref. 14) and b_A is a factor reflecting entropy change as defined in Eq. (7b) (Ref. 15).

Parameter→ ↓ element A	V_A (10^{-6} m^3)	H_A^{fuse} (kJ/mol)	$\Delta H_{A \text{ in } B}^{\text{interface}}$ (kJ/mol)	T_m^A (K)	$(\gamma V_A^{2/3})^{T=0}$ (10^{-3} J/mol)	b_A (10^{-7} J/K)
Ni	6.6	17.48	A=Ni, B=Si: −126 A=Si, B=Ni: −145	1726	0.75	−0.47
Ti	10.6	15.45	A=Ti, B=Si: −252 A=Si, B=Ti: −236	1943	0.92	−0.73
Pt	9.1	22.18	A=Pr. B=Si: −206 A=Si, B=Pt: −184	2042	0.98	−0.49
Si	12.1	50.50	-	1685	0.48	−0.96

ary energies, then the values calculated for the driving force for grain boundary amorphization along other grain boundaries are smaller.

Thus for the Ni-Ti system the model predicts interface amorphization; grain boundary amorphization in the Ti layer and absence of grain boundary amorphization in the Ni layer. These predictions agree with the experimental data[3,4] (see Table II).

B. Ni-Zr system

The results of the calculations for the Ni-Zr system are shown in Fig. 4. Qualitatively, the results obtained for Ni-Zr are similar to those for Ni-Ti. Hence, there is a driving force for interface SSA [Fig. 4(c)], there is no driving force for SSA along grain boundaries in the Ni layer [Fig. 4(d)], but there is a driving force for SSA along (high angle) grain boundaries in the Zr layer [Fig. 4(e)]. These results agree with the experimental data[18,19] (see Table II).

C. Cu-Y system

Another binary crystalline-crystalline system for which SSA has been observed, is Cu-Y.[6] The results of the calculations for the Cu-Y system are shown in Fig. 5. The model predicts a driving force for interface SSA in the Cu-Y system ([Fig. 5(c)] and a driving force for grain boundary SSA in the Y layer [Fig. 5(e)], but there is no driving force for grain boundary SSA in the Cu layer [Fig. 5(d)]. These predictions agree with the experimental data[6] (see Table II).

D. General discussion

In Table II a comparison is given of the predicted and experimental results on SSA in binary crystalline-crystalline systems. For all three systems to which the model has been applied there is a complete agreement between the experimental results and the predictions based on the model. Hence, the occurrence of SSA instead of CSS can be explained on a thermodynamic basis. There is no need to assume the existence of a kinetic barrier for the formation of the corresponding crystalline solid solution: the amorphous layer develops because it provides a larger gain in Gibbs free energy. However, it should be realized that the model as applied in this paper does not take into account the possibility of formation of a crystalline intermetallic compound.

VI. APPLICATION TO CRYSTALLINE-AMORPHOUS BINARY SYSTEMS

As indicated in Sec. III [below Eq. (17)], the model can in principle be applied equally well to crystalline-amorphous systems. A significant amount of experimental results about SSA in crystalline-amorphous systems is available regarding (transition) metal (crystalline)-silicon (amorphous) systems. The energy contributions essential for a thermodynamic description of SSA in these systems are calculated as a function of the composition of the amorphous (or crystalline solid solution) phase using the parameters given in Table II, for a unit cell of lateral area of 10×10 nm^2 and with a height equal to the sum of D_A (=10 nm) and D_B (=10 nm) (see Figs. 1 and 2). The product layer (SSA or CSS) is taken as 1 atom thick (defined as the interplanar spacing of the closed packed planes), representing the initial stage of the transformation. For each system considered, the temperature used in the calculations was taken as that of the heat treatment as applied in the corresponding experiments reported in the literature. The zero values of ΔG^f are defined with respect to a mechanical mixture of $\langle A\rangle$ and $\{B\}$.

As for the crystalline-crystalline systems, in the case of both interface and grain boundary SSA, the composition of the amorphous phase at the grain boundary is taken different from that at the interface.

A. Ni-*a*Si system

The results of the thermodynamic calculations for the possible SSA and CSS processes in a Ni-*a*Si system are depicted in Figs. 6(a)–6(c). The driving force for the formation of an one atom thick layer of an amorphous phase [modified Eq. (3a), see Sec. III below Eq. (17)] and a solid solution [modified Eq. (3b)] are given in Fig. 6(c) as a function of the Ni content of the product phase.

It follows from Fig. 6(c) that there is always a driving force for amorphization except for an amorphous phase of high Ni content. The formation of a CSS layer has a (relatively small) driving force within a range of Ni content from about 0.05 to 0.90. Clearly, in this concentration range the driving force for SSA at the interface is larger than that for the corresponding CSS at the interface. Although the Gibbs free energy of formation of the SSA layer [dashed line in Fig. 6(b)] is less negative than that of the corresponding CSS layer [full line in Fig. 6(b)], the formation of an amorphous

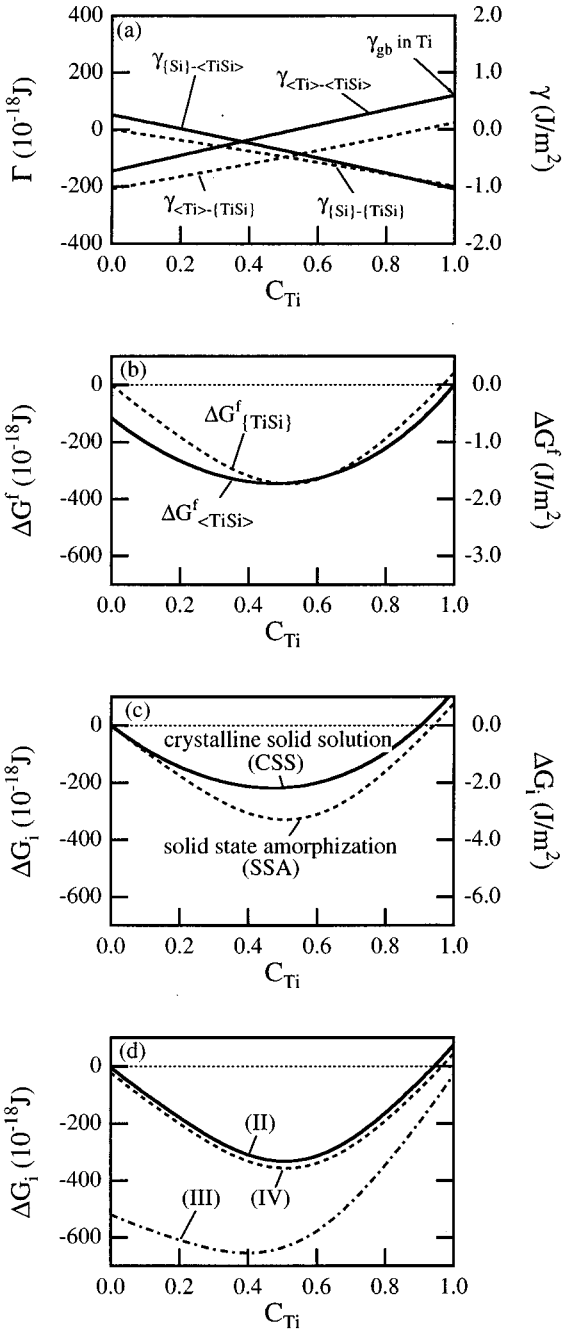

FIG. 7. Results of the thermodynamic model for solid-state amorphization (SSA) in the Ti-*a*Si system at 675 K. For details, see caption of Fig. 3.

phase is favored by the creation of an amorphous-amorphous interface [Fig. 6(a)]. Hence, the model predicts interfacial solid-state amorphization in the Ni-*a*Si system.

The driving forces for the formation of an amorphous phase along the interface and/or along the grain boundaries in the crystalline parent phase (here Ni; see the three cases II–IV considered in Sec. III and depicted in Fig. 2) are given in Fig. 6(d). Again, only the initial stages of interface amorphization and/or grain-boundary amorphization have been considered, i.e., the calculations pertain to a product layer of one atom thickness. Thus, also the composition of the amorphous phase at the grain boundaries is taken differently from that at the interface: the (initial) amorphous phase at the Ni grain boundary has a Ni content of about $c_{Ni} \cong 1$, whereas the Ni content of the amorphous phase at the interface is considered for $0 \leqslant c_{Ni} \leqslant 1$.

The driving force for only grain boundary SSA in the Ni layer is marginally negative at $C_{Ni}=1$ [i.e., $\Delta G_i > 0$; see curve III at $c_{Ni}=1$, in Fig. 6(d)]. Consequently, the driving force for only interface SSA [see curve II in Fig. 6(d)] is slightly larger than that for simultaneous interface and grain boundary SSA (with $c_{Ni} \cong 1$) in the Ni layer [see curve IV in Fig. 6(d)]. Therefore, only interface SSA is predicted for the Ni-*a*Si system. This result agrees well with the experimental data[20] (see Table III).

B. Ti-*a*Si system

The results of the calculations for the Ti-*a*Si system are depicted in Figs. 7(a)–7(d). Qualitatively, the results obtained for Ti-*a*Si are similar to those for Ni-*a*Si (cf. Figs. 6 and 7). Hence, the model predicts the occurrence of interface SSA in the Ti-*a*Si system.

However, in contrast with the Ni-*a*Si system, the driving force for grain boundary SSA in the crystalline Ti layer is positive [i.e., $\Delta G_i < 0$; curve III at $c_{Ti}=1$, in Fig. 7(d)]: hence, no nucleation barrier exists for grain boundary SSA in the Ti layer. Consequently the driving force for only interface SSA [see curve II in Fig. 7(d)] is smaller than that for simultaneous interface and grain boundary SSA (with $c_{Ti} \cong 1$) in the Ti layer [see curve IV in Fig. 7(d)]. Thus, both interface SSA and grain boundary SSA are predicted to occur in the Ti-*a*Si system. In the literature only interface SSA has been reported.[7]

C. Pt-*a*Si system

The results of the calculations for the Pt-*a*Si system at $T=300$ K are depicted in Figs. 8(a)–8(d). As follows from Fig. 8(c) there is always a driving force for amorphization, except for an amorphous phase of high Pt content. The same holds for the formation of a crystalline solid solution. The driving force for the formation of a CSS layer is larger than that of a SSA layer for a Si rich product layer ($c_{Pt} \leqslant 0.3$). In the concentration range $0.3 \leqslant C_{Pt} \leqslant 0.9$, the driving force for formation of a SSA layer exceeds that of the corresponding CSS layer. As the initially formed product phase will be probably one with a low Pt content [implying that the reaction proceeds by diffusion of Pt into the *a*-Si layers, $\Delta G_i < 0$, see Fig. 8(c)], rather than one with a high Pt content, the model suggests the formation of a CSS layer.

The driving forces for the formation at 300 K of an amorphous phase along the interface and/or grain boundaries in the crystalline sublayer (see the three cases II–IV considered in Sec. III and depicted in Fig. 2) are given in Fig. 8(d). The driving force for only grain boundary amorphization in the Pt layer is (marginally) negative for a Pt rich amorphous phase

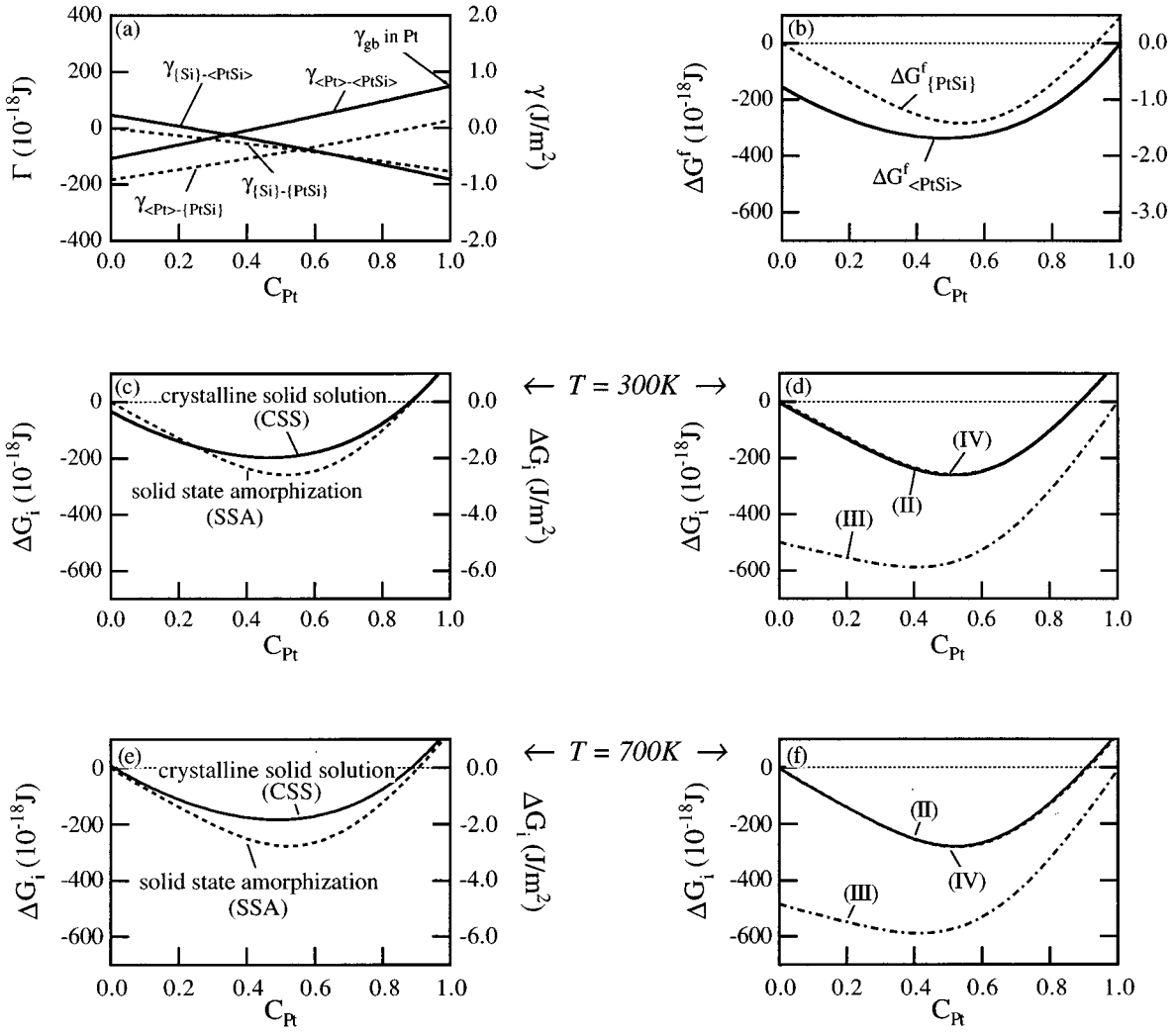

FIG. 8. Results of the thermodynamic model for solid-state amorphization (SSA) in the Pt-*a*Si system at 300 K. For details, see caption of Fig. 3. (e) and (f) are similar to (c) and (d) but hold for $T=700$ K.

[$\Delta G_i>0$; curve III at $c_{Pt}=1$, in Fig. 8(d)]. Consequently the driving force for only interface SSA [see curve II in Fig. 8(d)] is slightly larger than that for simultaneous interface and grain boundary SSA (with $c_{Pt}\cong 1$) in the Pt layer [see curve IV in Fig. 8(d)]. However, as already stated above it is likely that a CSS layer is formed rather than a SSA layer. Therefore at 300 K, only interface CSS is predicted to occur in the Pt-*a*Si system.

The results of the calculations for the Pt-*a*Si system at 700 K are depicted in Figs. 8(e) and 8(f). In contrast with the system at 300 K, now the driving force for the formation of an amorphous phase exceeds that of a crystalline solid solution up to $c_{Pt}\approx 0.9$ [Fig. 8(e)]. Hence, at 700 K interface SSA will occur in the Pt-*a*Si system.

The driving forces for the formation at 700 K of an amorphous phase along the interface and/or grain boundaries in the crystalline Pt layer are given in Fig. 8(f). In contrast with the results at 300 K, at 700 K no nucleation barrier exists for grain boundary SSA in the Pt layer [$\Delta G_i<0$, curve III at $c_{Pt}=1$, in Fig. 8(f)]. Consequently the driving force for only interface SSA [see curve II in Fig. 8(f)] is slightly smaller than that for simultaneous interface and grain boundary SSA (with $c_{Pt}\cong 1$) in the Pt layer [see curve IV in Fig. 8(f)]. Therefore at 700 K, both interface SSA and grain boundary SSA are predicted to occur in the Pt-*a*Si system.

The experimental data for the Pt-*a*Si system[21] show no trace of SSA below 475 K, whereas above 475 K, SSA is observed at the interface. The model predicts SSA to occur above $\approx$600 K. Grain boundary SSA in the Pt-*a*Si system has not been reported until now in the literature.

TABLE IV. Comparison between experimental observations and predictions of the model.

System	Ref.	Experimental observations	Predictions
Ni-aSi	20	at $T=675$ K - interface SSA - no grain boundary SSA in Ni	at $T=675$ K - interface SSA - no grian boundary SSA in Ni
Ti-aSi	7	at $T=675$ K - interface SSA - no grain boundary SSA in Ti	at $T=675$ K - interface SSA - grain boundary SSA in Ti
Pt-aSi	21	at $T=300$ K - no interface SSA - no data on grain boundary SSA available above $T=475$ K - interface SSA - no data on grain boundary SSA available	at $T=300$ K - no interface SSA, but formation of CSS. - no grain boundary SSA above $T=600$ K - interface SSA - grain boundary SSA

D. General discussion

In Table IV a comparison is given of predicted and experimental results on SSA in binary crystalline-amorphous systems. For the three systems considered the predictions concerning interface SSA agree well with the experimental results. Although grain boundary SSA is predicted to occur in the Ti-aSi and Pt-aSi systems, such observations have not been reported until now. This may be because in the studies concerned no search for this effect was conducted. Another possibility is that in the systems investigated no high angle grain boundaries occurred in the metal sublayers, and, as remarked in Sec. VI A, the driving force for grain boundary SSA is smaller for low angle grain boundaries; this effect may be important here because the calculated driving forces for grain boundary SSA are small as compared to those calculated in Sec. V for those cases where grain boundary SSA was indeed observed to occur.

VII. ESTIMATION OF THE MAXIMUM THICKNESS OF AN AMORPHOUS LAYER

A rough estimate for the maximum thickness of an amorphous layer formed by (interface) SSA can be made by using Eq. (26). Here, only the competition between the formation of a crystalline solid-solution phase and an amorphous phase is considered. The possible formation of a crystalline intermetallic compound, with a Gibbs free energy lower than that of the crystalline solid solution, is not taken into account. Also for this reason the calculated thickness can be considered an upper estimate of the maximum thickness of the amorphous product phase.

Results of the calculated maximum thickness of the amorphous phase, $D_{AB}^{\max}$, are shown as a function of the composition of the amorphous phase in Figs. 9(a) and 9(b). It follows that for the systems and temperatures considered in Secs. V and VI the value of $D_{AB}^{\max}$ ranges between 1 and more than 100 nm. According to the experiments reported in the literature, the amorphous product layer indeed attains in general a maximum thickness, before a crystalline phase forms.[2] The values calculated here agree well with the observed ones for the systems considered: see Table V. Thus, it is concluded that the apparent maximum thickness of the amorphous product layer can be explained on a thermodynamic basis.

In order to establish the temperature dependence of the thickness of the amorphous layer, $D_{AB}^{\max}$ has been calculated at a concentration c_A such that the total Gibbs free energy of the amorphous layer is approximately at minimum: see Figs. 10(a) and 10(b). Comparing Fig. 10(a) (crystalline-crystalline systems) and Fig. 10(b) (amorphous-crystalline systems) it follows that the crystalline-crystalline systems exhibit higher values of $D_{AB}^{\max}$. This is caused by the energy of an original amorphous-crystalline interface being lower than that of an original crystalline-crystalline interface (see Sec. IV). Further, the larger the Gibbs free energy of mixing of the system, the larger $D_{AB}^{\max}$ [see Figs. 10(a) and 10(b) and compare with Figs. 3(b), 4(b), 5(b), 6(b), 7(b), and 8(b)].

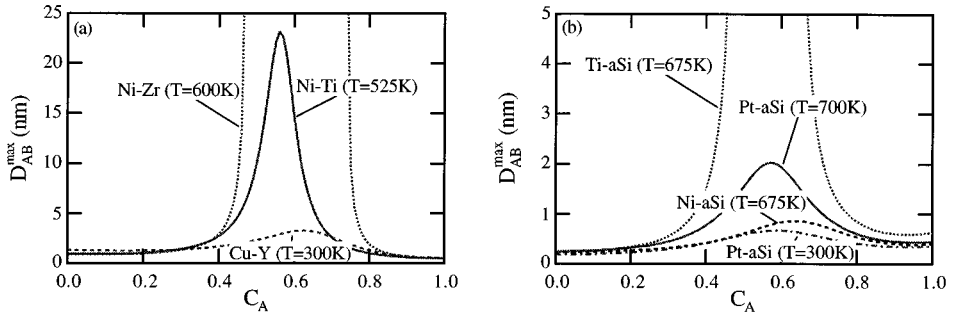

FIG. 9. The maximum thickness of the amorphous layer at the interface as a function of the molar fraction of A, c_A, in the amorphous product phase for (a) the A-B crystalline-crystalline systems Ni-Ti, Ni-Zr, and Cu-Y, and (b) the A-B crystalline-amorphous systems: Ni-aSi, Ti-aSi, and Pt-aSi.

TABLE V. Experimental observed and calculated maximum thickness of the amorphous layer.

		D_{AB}^{max} (nm)	
System	Ref.	Experimental observations	Predictions
Ni-Ti (525 K)	3	8 (c_{Ni}=0.5)	10 (c_{Ni}=0.5)
Ni-Zr (575 K)	22	≈100, formation of c-NiZr	∞
Cu-Y (300 K)	6	no experimental data	4 (c_{Cu}=0.62)
Ni-aSi (675 K)	23	≈1	1 (c_{Ni}=0.55)
Ti-aSi (675 K)	7	3.2 (c_{Ti}≈0.45)	4 (c_{Ti}=0.45)
Pt-aSi (700 K)	21	no experimental data	2

VIII. CONCLUSIONS

The thermodynamics of solid-state amorphization (SSA) at interfaces of binary systems can be well described by a model which takes into account energies of the original and developed interfaces. With an extension of this model for SSA to parent phases containing grain boundaries, also the thermodynamics of the formation of an amorphous phase at the grain boundaries can be described. Thermodynamic parameters used in the model can be well assessed using the approach due to Miedema.

The model predictions for the occurrence of interface SSA and of simultaneously occurring grain boundary SSA agree well with the available experimental results reported for binary crystalline-crystalline and crystalline-amorphous systems. For some crystalline-amorphous systems the predicted occurrence of grain boundary SSA cannot be confirmed or denied, because in the published experimental work grain boundary SSA was not reported.

It follows that in general an amorphous-crystalline interface has a lower energy than a crystalline-crystalline interface. It has not been realized until now that in particular this fact is decisive in favoring the formation of an amorphous instead of a crystalline solid solution. Thus, there is no need to invoke kinetic conditions to explain the occurrence of an amorphous phase. On this basis, also the experimentally observed maximum thickness of an amorphous product layer can be explained thermodynamically. The predicted values for this maximum layer thickness agree very well with the experimental results. As a side result of this work, the maximum thickness of the amorphous layer on the surface of a crystalline solid can be calculated.

ACKNOWLEDGMENTS

We are indebted to Dr. F. W. Schapink for critically reading the manuscript. The work described in this paper was made possible in part by financial support from the Netherlands Technology Foundation (STW).

APPENDIX

In this appendix it will be shown that

$$V_A^e \frac{G_{\langle A\rangle}}{V_A} + V_B^e \frac{G_{\langle B\rangle}}{V_B} + V_{AB}^e \frac{G_{\{AB\}}}{V_{AB}} = V_A^0 \frac{G_{\langle A\rangle}}{V_A} + V_B^0 \frac{G_{\langle B\rangle}}{V_B} + V_{AB}^e \frac{G_{\{AB\}}^f}{V_{AB}}, \quad \text{(A1)}$$

where $G_{\langle A\rangle}$, $G_{\langle B\rangle}$ and $G_{\{AB\}}$ are the Gibbs free energies of $\langle A\rangle$, $\langle B\rangle$ and $\{AB\}$, respectively; V_A, V_B, and V_{AB} are the molar volumes of $\langle A\rangle$, $\langle B\rangle$ and $\{AB\}$, respectively; V_A^0 and V_B^0 are the volumes of the phases before amorphization has occurred. V_A^e, V_B^e and V_{AB}^e are the volumes of the phases after amorphization has occurred. $G_{\{AB\}}^f$ is defined as [see above (2b)]

$$G_{\{AB\}}^f(c_A) \equiv G_{\{AB\}}(c_A) - c_A G_{\langle A\rangle} - (1-c_A) G_{\langle B\rangle}, \quad \text{(A2)}$$

where c_A denotes the mole fraction A in $\{AB\}$.

Assuming that both interface and grain-boundary amorphization occurs (situation IV as sketched in Fig. 2) and that the molar volumes of A and B do not change upon alloying [$V_{AB} = c_A V_A + (1-c_A) V_B$, with V_A and V_B as constants], the following reasoning can be made: define the volume of all A atoms in the amorphous phase at the interface as V_A^i, the volume of all B atoms in the amorphous phase at the interface as V_B^i; the volume of all A atoms in the amorphous phase at the grain boundary as V_A^{gb} and the volume of all B atoms in the amorphous phase at the grain boundary as V_B^{gb}. Thus,

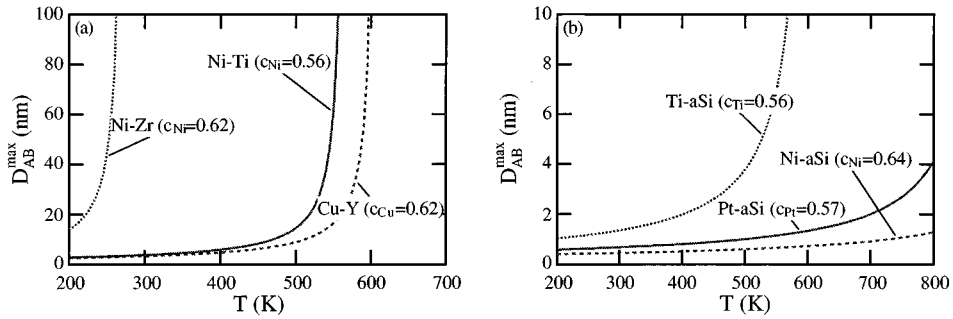

FIG. 10. The maximum thickness of the amorphous layer at the interface as a function of reaction temperature for (a) the A-B crystalline-crystalline systems Ni-Ti, Ni-Zr, and Cu-Y, and (b) the A-B crystalline-amorphous systems Ni-aSi, Ti-aSi, and Pt-aSi. For these calculations the molar fraction of A in the amorphous product phase has been fixed at the value corresponding with about the lowest Gibbs free energy of the amorphous phase.

$$V_A^0 = V_A^e + V_A^i + V_A^{gb}; \quad V_B^0 = V_B^e + V_B^i + V_B^{gb};$$

$$V_{AB}^e = V_{AB}^i + V_{AB}^{gb};$$

$$V_{AB}^i = V_A^i + V_B^i; \quad V_{AB}^{gb} = V_A^{gb} + V_B^{gb} \tag{A3}$$

and

$$G_{\{AB\}} = \frac{V_{AB}^i}{V_{AB}^e} G_{\{AB\}}^i + \frac{V_{AB}^{gb}}{V_{AB}^e} G_{\{AB\}}^{gb}, \tag{A4}$$

where $G^{i}_{\{AB\}}$ and $G^{gb}_{\{AB\}}$ are the Gibbs free energies of the amorphous phases at the interface and at the grain boundary, respectively. Defining c^{i}_{A} and c^{gb}_{A} as the molar fractions of A in the amorphous phase at the interface and at the grain boundaries respectively, it follows

$$c_A^i = \frac{V_A^i/V_A}{V_A^i/V_A + V_B^i/V_B}; \quad c_A^{gb} = \frac{V_A^{gb}/V_A}{V_A^{gb}/V_A + V_B^{gb}/V_B}. \tag{A5}$$

Substituting Eqs. (A2), (A3), (A4) and (A5) in the left-hand side of Eq. (A1) leads after some algebra to the expression at the right-hand side of Eq. (A1).

Note that in the above reasoning no values are given to V^{i}_{A} and V^{i}_{B} or V^{gb}_{A} and V^{gb}_{B}. Therefore by taking the volume of the amorphous phase either along the grain boundary or along the interface as nil, the above reasoning can be applied as well to the cases of only interface amorphization and only grain boundary amorphization, separately.

*Electronic address: benedictus@stm.tudelft.nl, bottger@stm.tudelft.nl

[1] R. B. Schwarz and W. L. Johnson, Phys. Rev. Lett. **51**, 415 (1983).

[2] W. L. Johnson, in *Materials Interfaces*, edited by D. Wolf and S. Yip (Chapman and Hall, London, 1992), Chap. 20.

[3] M. A. Hollanders, B. J. Thijsse, and E. J. Mittemeijer, Phys. Rev. B **42**, 5481 (1990).

[4] R. Benedictus, K. Han, A. Böttger, H. W. Zandbergen, and E. J. Mittemeijer, in *Proceedings of International Conference on Solid-Solid Phase Transformation*, Pittsburgh, 1994, edited by W. C. Johnson, J. M. Howe, D. E. Laughlin, and W. A. Soffa (Minerals, Metals and Materials Society, Warrendale, 1994), p. 1027.

[5] S-G Chang, J-L Lee, G-H Kim, and C-H Chun, J. Mater. Res. **10**, 1555 (1995).

[6] R. W. Johnson, C. C. Chan, and E. R. Ratner, Phys. Rev. B **40**, 8139 (1989).

[7] K. Halloway and R. Sinclair, J. Less-Common Met. **140**, 139 (1988).

[8] K. Binder, *Phase Transitions and Critical Phenomena* (Academic, London, 1986), Vol. 8, p. 35; S. Dietrich, *ibid*., Vol 12, p. 2.

[9] M. Gerl and P. Guilmin, Solid State Phenomena **3**, 215 (1988).

[10] H. W. Wang, H. Y. Bai, Y. Zhang, H. Chen, and W. K. Wang, J. Appl. Phys. **73**, 7217 (1993).

[11] F. R. de Boer, R. Boom, W. C. M. Mattens, A. R. Miedema, and A. K. Niessen, in *Cohesion in Metals: Transition Metals Alloys* (North-Holland, Amsterdam, 1988), Chap. 2.

[12] D. Turnbull, Contemp. Phys. **10**, 473 (1969).

[13] A. W. Weeber, J. Phys. F: Met. Phys. **17**, 809 (1987).

[14] A. R. Miedema and F. J. den Broeder, Z. Metallkde. **70**, 14 (1979).

[15] F. R. de Boer, R. Boom, W. C. M. Mattens, A. R. Miedema, and A. K. Niessen, in *Cohesion in Metals: Transition Metals Alloys* (North-Holland, Amsterdam, 1988), Chap. 4.

[16] R. H. Ewing, Philos. Mag. **25**, 779 (1972).

[17] F. Spaepen, Acta Met. **23**, 729 (1975); F. Spaepen and R. B. Meijer, Scripta Met. **10**, 257 (1976).

[18] W. J. Meng, C. W. Nieh, E. Ma, B. Fultz, and W. L. Johnson, Mater. Sci. Eng. **97**, 87 (1988).

[19] A. M. Vredenburg, J. F. M. Westendorp, F. W. Saris, N. M. van der Pers, and Th. H. de Keijser, J. Mater. Res. **1**, 774 (1986).

[20] W. H. Wang, H. Y. Bai, and K. W. Wang, Mater. Sci. Eng. **A179**, 229 (1994).

[21] D. M. Walker, Phys. Status Solidi A **94**, 77 (1986); M. O. Aboelfotoh, A. Allesandri, and F. M. d'Heurle, Appl. Phys. Lett. **49**, 1242 (1986).

[22] W. J. Meng, C. W. Nieh, and W. L. Johnson, Appl. Phys. Lett. **51**, 1693 (1987).

[23] E. Ma, W. J. Meng, W. L. Johnson, and M-A. Nicolet, Appl. Phys. Lett. **53**, 21 (1988).